Multi-spectral Imaging of La Casa de las Golondrinas Rock Paintings

Research Year: 2000
Culture: Maya
Chronology: Pre-Classic, Proto Classic, and Early Classic
Location: Antigua Valley, Guatemala
Site: The House of the Swallows

Table of Contents

The Final Report

La Casa de las Golondrinas (The House of the Swallows), located in the Antigua Valley, Guatemala, is the largest rock art site in the Guatemalan Highlands. Like other painted rock art sites in the highlands, the site is at a sacred location near water. In Mesoamerican thought, caves, which often have streams within, are entrances to mountains and symbolically unite earth and water elements. Along with mountain peaks, they are the most important natural shrines in Mesoamerica. Places from which water emerges like caves also represent the female attributes of creation and fertility. Devotion to the deities, who monitored these aspects of life, could have taken place at Las Golondrinas.

Golondrinas may have been a religious and political landmark for thousands of years. Indeed, pottery that dates to the Preclassic (1000 B.C.-300 A.D.), Early Classic (300-600 A.D.), Protohistoric (1300-1500 A.D.) and Postconquest periods has been found at the site. Many of the 105 paintings recorded at the site so far, based on stylistic and thematic criteria, appear to pertain to late in the Postclassic period. Numerous abstract and fantastic motifs, however, have uncertain themes and styles admitting to the possibility that they date to earlier times.

Spreading over a 500-meter distance on a 30-meter tall tuff wall are areas with clusters of paintings. Delineated with red paint are Postclassic glyphs and shields, images of political domination from an external Mexican polity.

In an eastern section is a round 10-centimeter solar sight cut into a rock boulder about 2.4 meters above the ground surface (Figure 1, shown below). Sun images are lined up along a western wall perpendicular to the sight suggesting that these images match positions of the sun (or possibly other astronomical bodies) at different times of the year. An emphasis in solar imagery exists in this area of the site with human-like figures with rayed heads and murals including prominent suns.

Figure 1. Photograph of the sighting hole in Area C.

In another area a well-preserved painting is a group of animals appearing to cascade down the face of the rock (Figure 2, shown below). In this mélange are terrestrial and aquatic animals in frontal and profile poses. The complex composition of multiple animals fitted one into the other is unusual at Golondrinas. The painting expresses an animation unlike others at the site and suggests a theme concerning the fecundity of animal life if not creation itself.

Figure 2. Photograph of painting 16 in Area A.

Multispectral imaging is a non-invasive preservation technique that can enhance faded details and differentiate between pigments used in paintings. The fundamental techniques of archaeological multispectral imaging come from the remote imaging of the Earth from space. For archaeological imaging, this distance is measured, at most, in a few meters rather than the hundreds of kilometers from a space-based sensor.

In order to form a multispectral image cube, images of the same scene, each at a different wavelength, are stacked on top of each other. This multispectral image cube may be processed to reveal image information associated with spectral differences between images, which may not be apparent in the individual images. In addition, individual images may show increased contrast due to a relatively narrow bandwidth around the image center wavelength.

For the Golondrinas data, each image cube contains ten wavelengths: 450, 500, 550, 600, 750, 800, 900, and 1000 nm each with a bandwidth of 40 nm. A Kodak Megaplus 4.2i/10 was used to produce the digital image files, which were recorded in the field on a computer hard disk and CD-ROM. There were 32 drawings imaged and some drawings were imaged in multiple parts leading to 57 image cubes containing 570 digital images.

In several cases, the multispectral images revealed details not easily seen by eye. For example, images in the infrared (Figure 3b) clearly showed a sun-like image with rays (Area B #8), especially in the upper-left quadrant. The color photograph (Figure 3a) also hints at these rays. The rays are not seen in images at 450 and 500 nm. A false color composite image (Figure 3c) was constructed from the 500, 900, and 1000 nm images in an effort to enhance the rays.

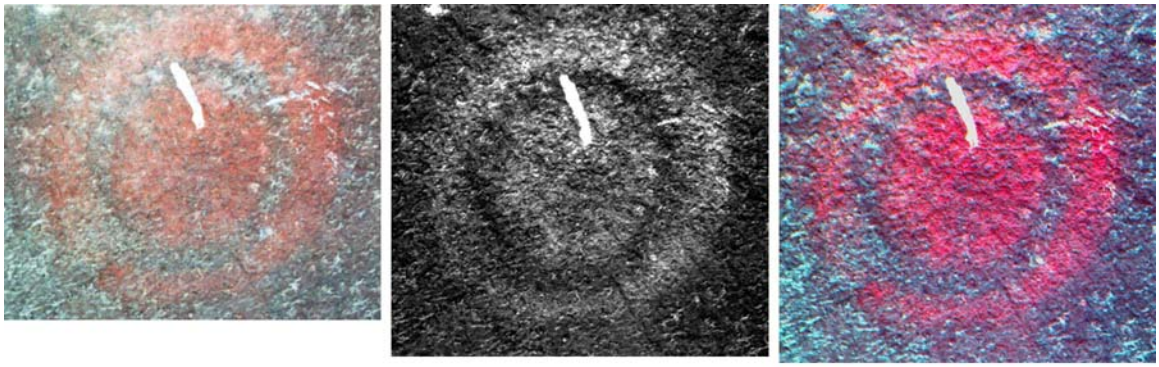

(a) (b) (c)

Figure 3. Images of drawing 8 in Area B: (a) color photograph, (b) digital image at 1000 nm, and (c) false color image comprised of digital images at 500, 900, and 1000 nm.

Surprisingly, the rays seem to fade and, if present, appear in a darker red color. The two different shades of red give rise to the possibility of different pigments. Spectral classification techniques likely will aid in the pigment identification and the possible existence of the rays.

Two digital images of a sun are shown in Figure 4, below. Note that the pigment has faded at 1000 nm (Figure 4a) but is clearly visible at 550 nm (Figure 4b). Most pigments, including those at Golondrinas, tend to become transparent in the infrared as illustrated by Figure 4. The pigment spectral characteristics of the pigments in Figure 3, however, are different in that they appear to become opaque in the infrared at 1000 nm. It is expected that further image processing and spectral classification will aid in the identification of the pigment detail and spectral characteristics of the Golondrinas drawings.

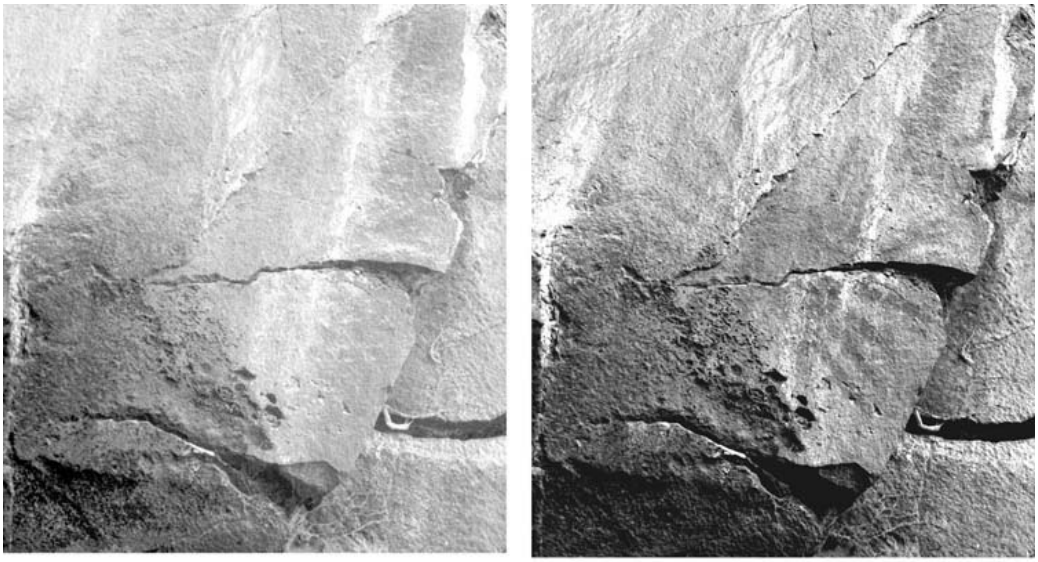

Figure 4. Painting 10 in Area C (a) at 1000 nm and (b) at 550 nm.

The multispectral imaging of the La Casa de las Golondrinas paintings posed several interesting challenges. Because the site is open to the environment, the images were obtained using natural light. This often made it difficult to track the variations in lighting caused by the sun's position and clouds. An attempt was made to select appropriate times during the day for each drawing. Also, drawings were located from ground level to over 6 meters above the ground. This often made head-on imaging difficult or impossible. In one case (Area B #1), a 6-meter scaffold was fabricated to allow detailed imaging (Figure 5, shown below).

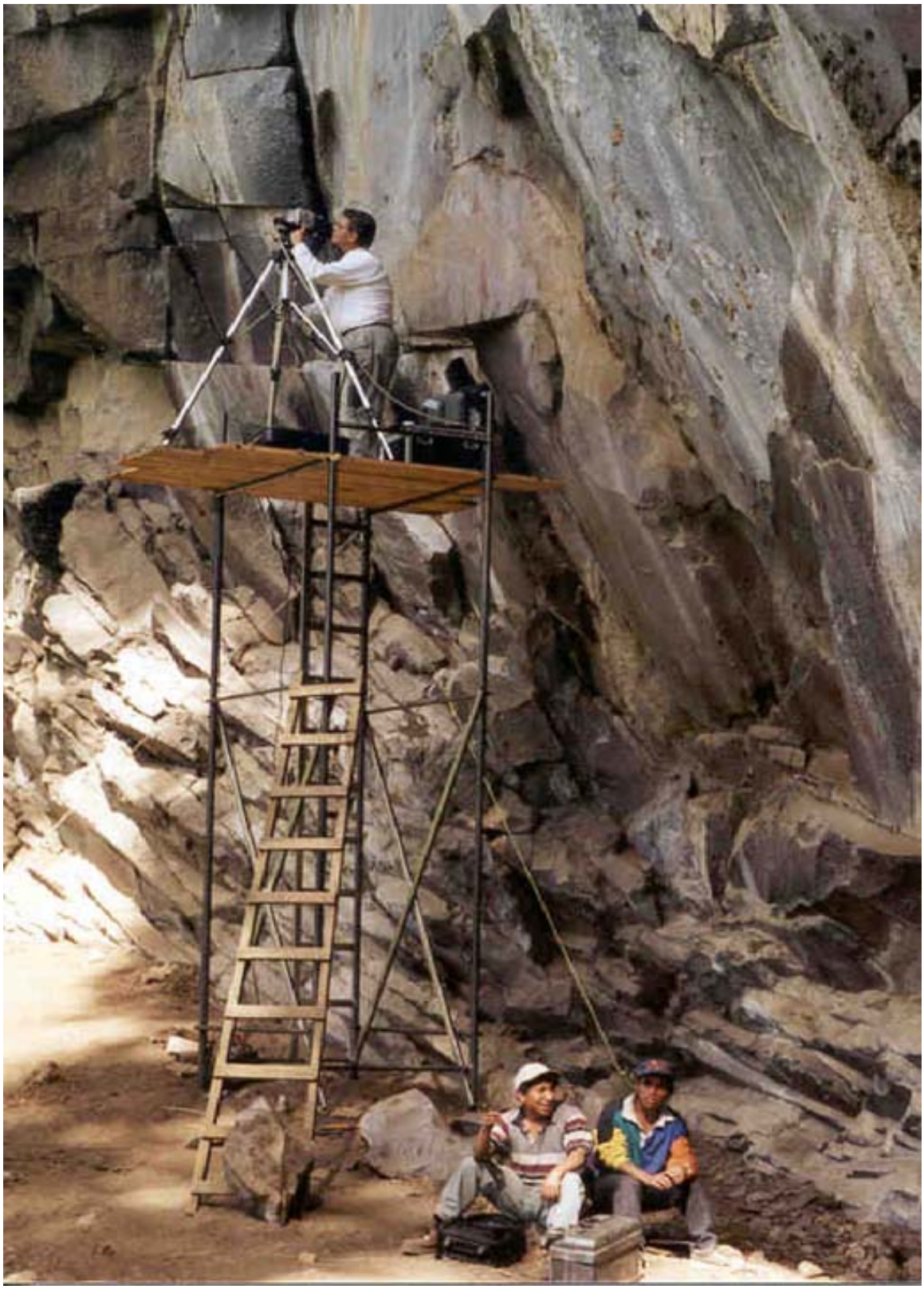

Figure 5. Gene Ware working on the 6-meter scaffolding at La Casa de las Golondrinas.

List of Figures

The Technical Report

Multispectral Imaging

The application of multispectral imaging to archaeology is relatively new. An archaeological multispectral imaging system has been engineered and fabricated at Brigham Young University to meet the needs of this new area of research. This report describes the detail of this multispectral imaging system as used to image the rock paintings at Golondrinas in Guatemala.

Figure 1a. Typical setup of the multispectral imaging equipment at Golondrinas.

A typical multispectral imaging setup at Golondrinas is shown in Figure 1a. The camera, filter wheel, and lens are at the right while the camera control computer is at the left. Umbrellas are used to shield the equipment from direct sunlight. Direct sunlight on the camera increases the temperature of the internal imaging array which leads to an increased noise level in the image. Readability of the computer display is improved by the umbrella shade as well as reducing the temperature of the computer.

This system has been used effectively to obtain multi-spectral images of a wide range of archaeological artifacts including ancient documents, carbonized scrolls, murals, drawings, rock art, and ceramics. The imaging system has been reliably transported to and used in environments ranging from the laboratory to museums, the jungle, and caves.

Multispectral Equipment

The basic elements of this multispectral imaging system include a digital camera, a filter wheel, optical filters, a lens, and a camera control computer. These elements will be briefly discussed herein. A more complete discussion, presented by Ware, Chabries, and Baker (2001), is given in Appendix A.

Figure 2a. Closeup of the Kodak Megaplus 4.2i/10 camera and filter wheel used at Golondrinas.

The core element of the imaging system is the Kodak Megaplus 4.2i/10 digital camera shown in Figure 2a, above.[1] The 2029x2044 pixel imaging array of this camera is coated to provide response from 200 nm through 400 nm in the ultraviolet (UV) in addition to the normal response from 400 nm into the near infrared (NIR) at 1100 nm. This yields a 5-to-1 range in wavelength which is considerably greater than cameras used for normal color photography. The camera also has a 10-bit dynamic range which corresponds to a film density of greater than 3.

Optical interference (Schott) filters are used to restrict the spectral bandwidth of the camera to a desired wavelength range. A wide selection of these filters is available from the UV through the NIR. Filters for the Golondrinas project were selected from a set of seven visible filters and a set of six NIR filters, both of which were at a bandwidth of 40 nm. The filter transmission curves for these filters, manufactured by Thermo Corion Optical Filters, are given in Figure 3a, shown below. Notice that they cover the 400 through 1000-nm spectral region with small 10-nm interstitial gaps. A 62-filter set with a 10-nm bandwidth (manufactured by Andover Corporation) and a visible tuneable filter (manufactured by Cambridge Research Instrumentation, Inc.) are also available for detailed hyperspectral imaging.

[1] The Kodak Motion Analysis Systems Division has been acquired by Roper Scientific MASD, Inc.

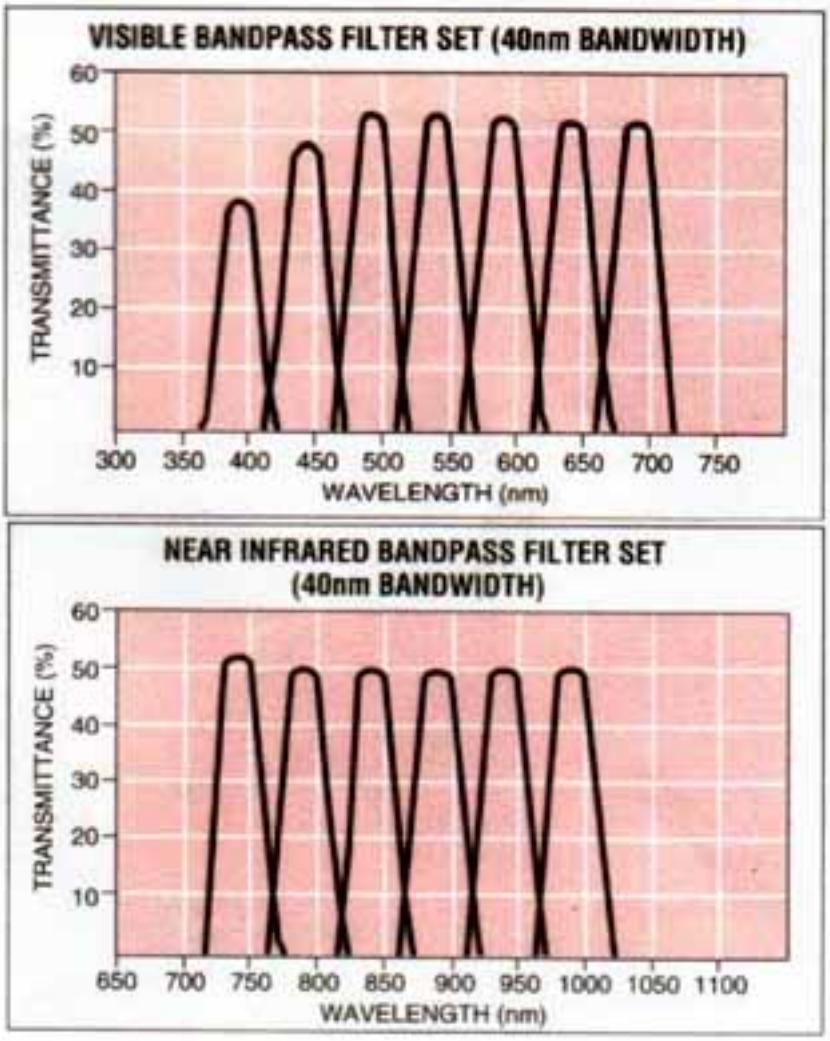

Figure 3a. Transmission curves for the Corion 40-nm visible bandpass filter set (top) and near infrared bandpass filter set (bottom) (Corion Optical Filters and Coatings, 1994 Catalog).

On-site tests were conducted at Golondrinas to determine the specific filters to be used. The testing involved determination of pigment spectral resonances and reflectance as well as a consideration of the wavelengths required for pigment spectral classification. No narrow-band pigment spectral resonances were observed with the test drawing allowing the use of filters with a 40-nm bandwidth. Ten wavelengths were selected: 450, 500, 550, 600, 650, 700, 750, 800, 900, and 1000 nm.

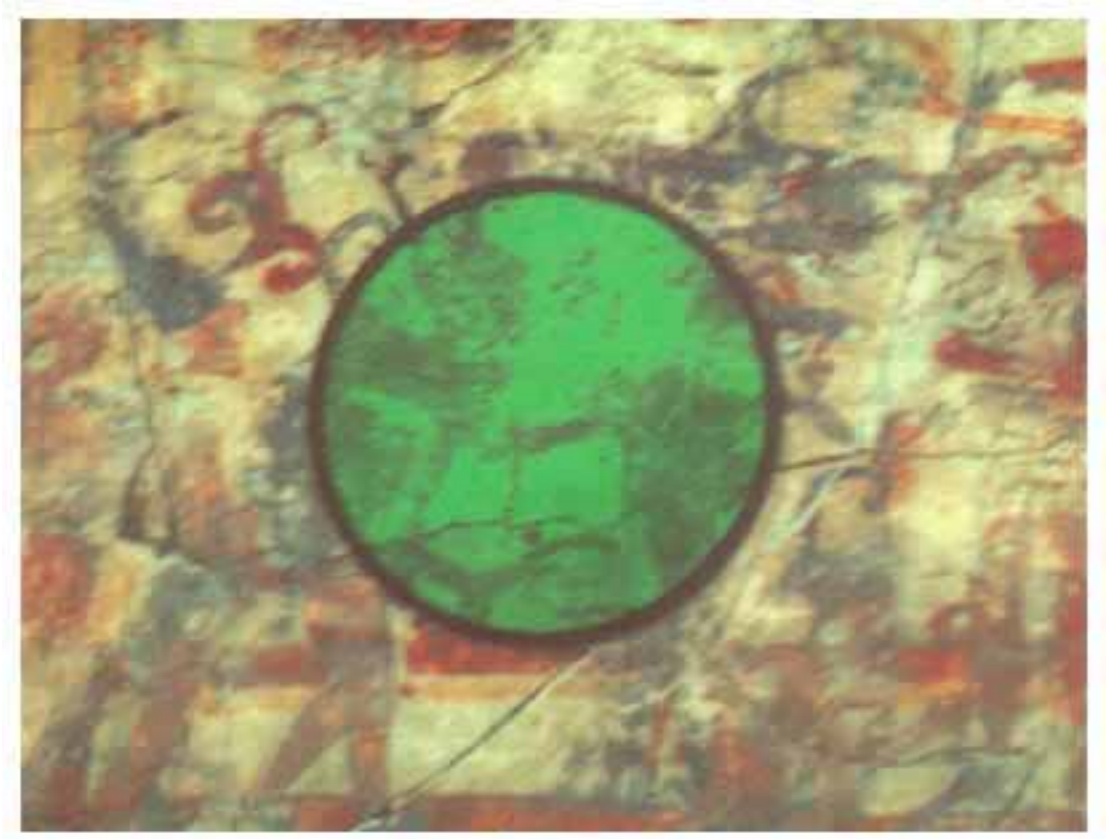

Figure 4a. An Andover 530 nm (green) filter.

A typical 2-inch filter is shown in Figure 4a. This particular filter is centered at 530 nm (green). Note that the image within the filter ranges from light green through dark green with all other colors filtered out. The camera converts this green light into a gray-scale image which records in intensity of the green filtered light. A similar process occurs for each filter used to produce the multi-spectral image set.

Rapid filter selection is provided by a filter wheel which can move the selected filter into position under remote control. The filter wheel in Figure 2a is the thin black disk located in front of the camera. The selected filters were mounted in a filter wheel similar to the one shown in top of Figure 5a, below. The front of the filter wheel provides a standard Nikon lens mount. The thickness of the filter wheel was designed to provide the proper focal length for the lens. Nikon 105 mm and 55 mm lenses were used as appropriate for the particular imaging requirements.

Figure 5a. Filter wheel and lens (top), and filter wheel interior (bottom).

The interior of the filter wheel showing the filter mounting positions is illustrated at the bottom of Figure 5a. The filter wheel used at Golondrinas contained 12 filter positions instead of the 14 positions shown in Figure 5a, but otherwise was identical. A belt (not visible) connects the wheel to a small external DC motor which is used to rotate the selected filter into place.

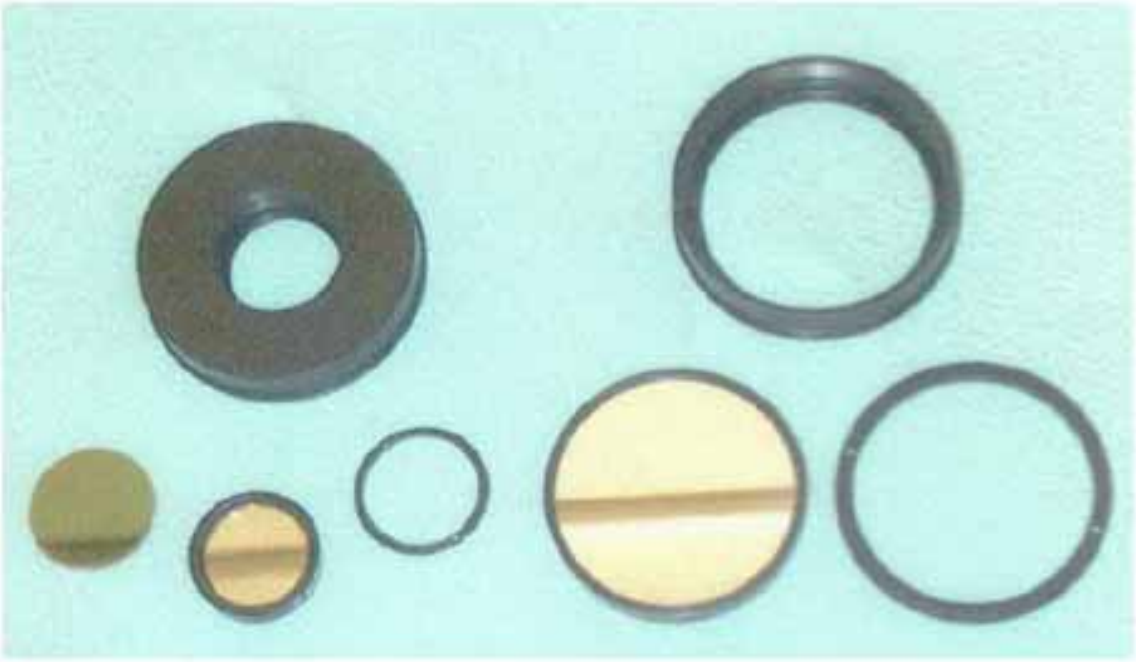

Figure 6a. Filter wheel mounting hardware.

The filters are mounted into the filter wheel using hardware adapters specific to the filter to be installed. Both 1-inch and 2-inch filters can be accommodated. This adapter hardware is illustrated in Figure 6a, above. Shown on the left is a 1-inch adapter with typical 1-inch filters. Shown on the right is a 2-inch adapter with a typical 2-inch filter.

Figure 7a. System control and data storage computer.

The camera is controlled by the computer shown in Figure 7a, above. A PCI-bus interface card is installed in the computer and connected to the camera with a SCSI-3 digital cable. The computer controls all functions of the camera through specialized software and transfers the digital image data to the computer hard disk for storage. The computer software also provides for automatic metadata storage which identifies the camera settings and filter in use. This computer also contains a removable hard-drive and a CD-writer (on the right side) for data storage and backup in the field.

The lunch-box configuration of the computer is necessary because computer-camera interfaces other than a PCI-bus interface have not been available. Laptop computers typically do not have a PCI slot (unless a docking station is used) and so cannot be used to operate the camera. A laptop-camera interface is currently under development and should allow laptops to be used in the future.

Image Processing

Image processing was not performed in the field at Golondrinas. The multispectral images were reviewed daily, checked for integrity, and backed up on CD. Techniques available with Adobe Photoshop were used to judge the quality of the images. It is expected that spectral classification techniques will be applied to the Golondrinas corpus to provide pigment differentiation and image enhancement. The theoretical foundation for this algorithm, presented by Martin and Ware (2001), is given as Appendix B.

Current image processing techniques which can be applied to the Golondrinas corpus include principle component analysis, transformations, image differencing, and spectral classification (Ware *et al*., 1999, 2000, 2001). Spectral classification has been effectively used with the Naj Tunich data set to separate pigments and is expected to provide significant results at Golondrinas.

As indicated above, (Multispectral Equipment) test images were obtained to determine the filter wavelengths to be used. This process is currently subjective, but special software, suitable for field operation, is being developed to quantify this decision. Also, the camera control software is being updated to allow more automatic operation and increased metadata capability.

Conclusions

The Brigham Young University multispectral imaging system effectively imaged the rock art drawings at Golondrinas. The project has provided significant insight into the techniques required to carryout rock art imaging under outdoor conditions including issues of access, calibration, and lighting (Robinson and Ware, 2001). Both equipment modifications to the system and software improvements have resulted. It is expected that laboratory analysis of the data will provide additional system improvements as well as significant understanding of the Golondrinas rock art.

Acknowledgments

This research project was supported by a grant from the Foundation for the Advancement of Mesoamerican Studies, Inc., (FAMSI). The Naj Tunich multispectral research was supported by grants from FAMSI, and the Center for Advanced Study in the Visual Arts of the National Gallery of Art.

The mechanical design of the filter wheel was done by Dean Shaeffer of Space Dynamics Laboratory, Logan, Utah, and Robert Perry of the BYU Research Machine Shop. Robert also led in the filter wheel fabrication, and in the design and fabrication of associated system hardware. The custom camera control software was written by Craig Lindstrom of eSage, Pleasant Grove, Utah.

All images are used by permission of Brigham Young University, Provo, Utah.

List of Figures

Sources Cited

Robinson, Eugenia J. and Gene A. Ware

2001 "Multi-spectral Imaging of La Casa de las Golondrinas Rock Paintings." Final Report submitted to FAMSI.

Ware, Gene A., Douglas M. Chabries, and Doran J. Baker

2001 "Multispectral Imaging for Archaeology." *SCI 2001: 5th World Multiconference on Systemics, Cybernetics and Informatics,* XIII:263-267.

Corion Corporation

1994 *Corion Optical Filters and Coatings,* Catalog, Corion Corporation, Franklin, Massachusetts. pp. 110-111.

Martin, Curtis E. and Gene A. Ware

2001 "Unsupervised Clustering for Data Reduction and Analysis of Multispectral Archaeological Images." *SCI 2001: 5th World Multiconference on Systemics, Cybernetics and Informatics,* XIII:257-262.

Ware, Gene A. and James E. Brady

1999 "Multispectral Analysis of Ancient Maya Pigments: Implications for the Naj Tunich Corpus," in *Center 19: Record of Activities and Research Reports June 1998-May 1999.* Washington D.C.: National Gallery of Art, Center for Advanced Study in the Visual Arts.

Ware, Gene A., Douglas M. Chabries, Richard W. Christiansen, and Curtis E. Martin

2000 "Multispectral Document Enhancement: Ancient Carbonized Scrolls." *Proceedings IEEE 2000 International Geoscience and Remote Sensing Symposium,* VI:2486-2488.

Ware, Gene A., Douglas M. Chabries, Richard W. Christiansen, James E. Brady, and Curtis E. Martin

2000 "Multispectral Analysis of Ancient Maya Pigments: Implications for the Naj Tunich Corpus." *Proceedings IEEE 2000 International Geoscience and Remote Sensing Symposium,* VI:2489-2491.

Ware, Gene A., James E. Brady, and Curtis E. Martin
2001 "Multispectral Imaging and Spectral Classification of Naj Tunich Pigments." *PICS 2001: Proceedings of the 54th Annual Conference of the Society for Imaging Science and Technology,* 22-25 April 2001, pp. 211-214.

Ware, Gene A., James E. Brady and Curtis E. Martin
2001 "Multispectral Imaging and Spectral Classification of Naj Tunich Pigments," *PICS 2001: Proceedings of the 54th Annual Conference of the Society for Imaging Science and Technology,* Quebec, Canada, April 22-25, 2001.

Kirkland, John S., Doran J. Baker, and Gene A. Ware
2001 "Principal Component Data Fusion of Infrared Telescope Multi-Spectral Images of the Galactic Center." *SCI 2001: 5th World Multiconference on Systemics, Cybernetics and Informatics,* XIII:251-256.

Wilson, Terry A.
2001 "Adaptive Multivariate Clustering Technique for Archaeological Pigment Classification."*SCI 2001: 5th World Multiconference on Systemics, Cybernetics and Informatics,*XIII:268-272.

Multi-spectral Imaging of La Casa de las Golondrinas Rock Paintings

Appendix A. Multispectral Imaging for Archaeology *by Gene A. Ware, Douglas M. Chabries, Brigham Young University; and Doran J. Baker, Space Dynamics Laboratory, Logan, Utah*

Table of Contents

Abstract

Multispectral imaging has been used extensively in Earth remote sensing. Recent application to ancient documents, murals, and archaeological artifacts, however, has led to exciting discoveries. In an archaeological setting, the remoteness is measured in hundreds of centimeters rather than hundreds of kilometers, and has more to do with hot, humid jungles than the environment of space. Except for differences imposed by the external surroundings, however, the measurement techniques are similar as are the data fusion methods employed in the analysis of the resulting images.

Multispectral imaging techniques are archaeologically important because differences between images at distinct wavelengths reveal detail and characteristics not clearly visible with conventional imaging methods. Not only can this lead to exciting archaeological discoveries, but it also is a technologically modern conservation technique for the preservation of ancient art forms for future scholarly study.

At Brigham Young University, multispectral imaging began with prototype multispectral imaging equipment used at Bonampak, Chiapas, México as part of a 1995-1996 Yale University expedition sponsored in part by the Getty Grant Program and the National Geographic Society (Miller, 1997). While the primary Bonampak imaging results included infrared video (1-2 µm), infrared film, and color film, the need for a modern archaeological multispectral imaging system was evident. This archaeological multispectral imaging system is described herein.

Multispectral Imaging

Multiple images of the same scene, each at a different wavelength, may be structured as an image cube where the images are stacked one on top of another. Looking down through the image cube there is a sequence of pixels each at the same physical location but differing in wavelength. When properly calibrated, such a sequence of pixels defines a spectral reflectance vector, $\mathbf{x}_{ij}$, where the indices specify the spatial location.

The term "multispectral" is commonly used to describe an image cube containing tens of different wavelengths each with a bandwidth on the order of 100-4000 nm (Belokon *et al.*, 1977). On the other hand, "hyperspectral" is typically used to describe image cubes with hundreds of wavelengths and bandwidths on the order of 10 nm. The imaging equipment described herein lies between these two definitions, but will be described as multispectral.

Archaeologists frequently discover artifacts that contain much more information than can be detected with the human eye. This is particularly true of inscriptions or paintings on ceramic vessels, temple walls, and caves. For example, painted texts in Maya caves are among the rarest of these contexts with only five sites currently known. Because these caves were considered sacred features in the ancient Maya landscape, the inscriptions may deal with esoteric beliefs and fundamental tenets of Maya religion that are not recorded elsewhere. The decipherment of these texts through multispectral imaging and analysis will provide important insights into Maya culture.

Imaging System Requirements

Important archaeological sites are often located at remote locations, are arduous to reach, and are environmentally difficult for operation of sensitive optical and electronic equipment. As an example, the topography of the cave at Naj Tunich, located in the jungle of Guatemala, is expansive both in the cross-section of its passages and in the extent to which the passages penetrate the limestone. Operation as deep as one kilometer into the cave required the camera, lighting, and associated computer hardware to be operated from a marine battery which was recharged with a generator outside of the cave. The cave atmosphere is

cool but very humid and acidic placing additional stress on the equipment. Other locations may be hot, dry, and exposed to direct sunlight such as the rock art at Golondrinas, México. In addition, it was desired to image ancient documents in a laboratory setting in the ultraviolet through the near infrared. To meet these needs, the multispectral system should exhibit the following characteristics:

1. The system should be relatively light, small, and rugged for ease of transportation by aircraft, four-wheel drive vehicles, and portage.
2. The system must operate from a variety of unstable electrical power sources including portable generators and batteries.
3. Critical system components must be easily repaired or replaced in the field.
4. The system must be able to record the image data on CD (or other non-volatile media) in the field.
5. The camera should be a high resolution digital imager with response from 200 nm in the ultraviolet through 1000 nm in the near infrared.

The basic system components of the multispectral system include a digital camera, a set of filters capable of selecting the appropriate image wavelength, a lighting source, and a controlling computer. Operating under computer control, the camera and filters form a multispectral imaging system capable of producing multispectral image sequences from the ultraviolet into the near infrared. These components will be individually discussed below.

This system has been successfully used by Brigham Young University at a variety of locations including Dumbarton Oaks (Washington, D.C.), the National Museum of Guatemala and Museo Popol Vuh (Guatemala City, Guatemala), Cueva de las Pinturas and Naj Tunich (Maya caves in the Petén, Guatemala), Tepantitla (Teotihuacán, México), Monte Albán (Oaxaca, México), and the American Center of Oriental Research (Amman, Jordan).

Digital Camera

After a review of available high-resolution digital cameras, a scientific-grade Kodak digital camera[1] was selected. This Megaplus 4.2i/10 camera provides a spatial resolution of 2029x2044 light-sensitive pixels with a 10-bit (60 dB) dynamic range. The intrinsic silicon sensor array responds to wavelengths of 400 nm through 1000 nm as shown by the typical response curve of Figure 1, below. The sensor array was coated with an organic lumigen compound to extend the short wavelength response to 200 nm with a quantum efficiency of about 10

[1] The Kodak Motion Analysis Systems Division has been acquired by Roper Scientific MASD, Inc.

percent. The resulting scientific grade 2 sensor array contained only three defective pixels, two of which were adjacent.

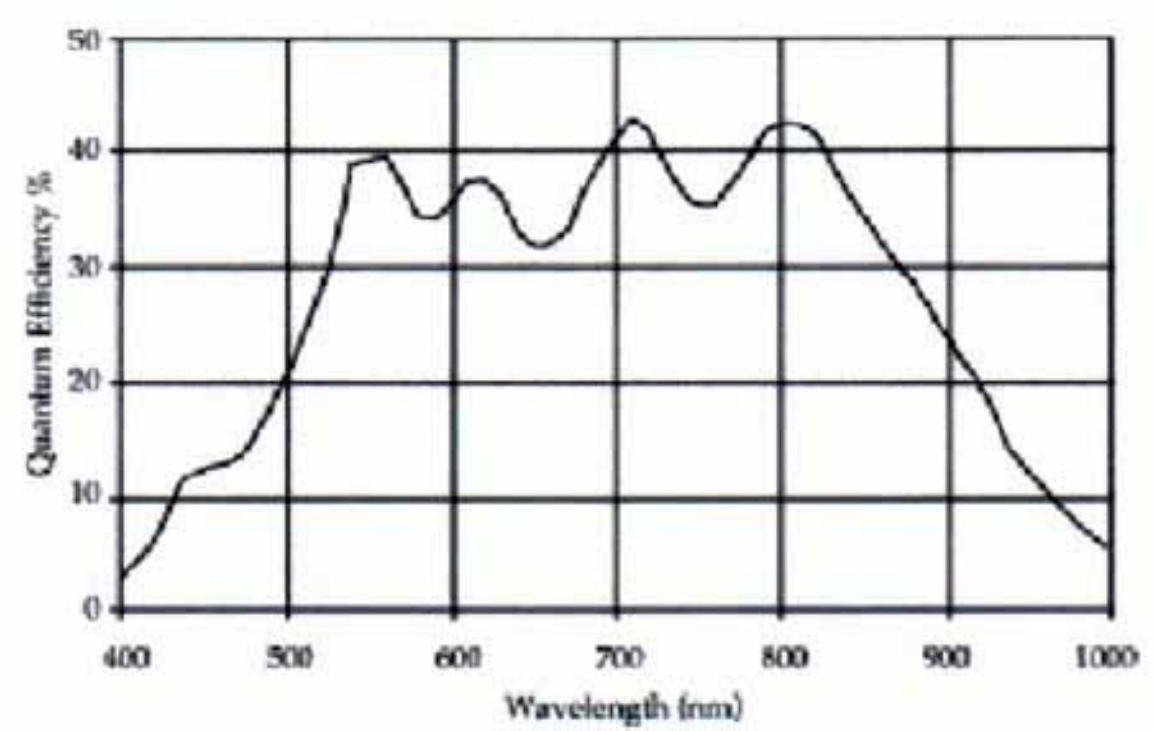

Figure 1. Typical response of the Kodak 4.2i sensor array. Curve by Roper Scientific MASD, Inc.

The sensor array size is 18.5x18.5 mm with 9x9 µm unity fill ratio pixels with a 9 µm center-to-center spacing.

The camera includes a mechanical shutter with exposure settings of 10 through 100,000 ms making possible high-speed image capture without vignetting. The shutter and sensor array are close to the front of the camera providing sufficient space to insert optical filters between the camera and the lens. The electronic pixel transfer rate is 10 mHz yielding a frame rate of 2.1 fps not including exposure time and computer image transfer time.

A PCI DV digital video camera interface by Engineering Design Team, Inc., (EDT) was chosen for the camera-computer link. This PCI bus card was selected because it used the computer memory to store the image which requires about 8 MByte for 10-bit pixels stored in a 16-bit format. A software library provides computer control of the camera exposure time, gain (0–24 dB), and black level. A custom program was written to provide both camera control and ancillary control for equipment such as filter wheels, electronic filters, and XY positioning tables.

Image data were recorded on the hard drive of the control computer. These data were regularly transferred to compact disks (CDs) on site using the control computer's CD writer.

Optical Filters

Image wavelength selection is provided by highly selective optical interference filters. Both fixed and tunable optical filters are available. The selected fixed optical interference (Schott) filters include matched sets from Andover Corporation covering wavelengths of 400 nm through 1050 nm in 10 nm steps (62 filters) with an optical bandwidth of 10 nm, and 14 filters from Thermo Corion Optical Filters centered from 400 nm to 1050 nm in 50-nm increments with an optical bandwidth of 40 nm. Both filter sets are blocked in the ultraviolet and infrared outside of the filter bandpass. Physically, the filters are 50.8 mm in diameter to minimize vignetting. A matched set of ten fixed ultraviolet filters (25.4 mm diameter) is also available.

These fixed interference filters can be mounted in a filter wheel with provision for automatic computer-controlled filter selection. Two filter wheels, one with 12 positions and one with 16 positions, were fabricated. These filter wheels are rotated by a small DC motor and have internal position registration sensors for automatic filter positioning and identification. Manual filter adapter rings are also available for mounting a filter in front of the lens. An on-site evaluation is performed to ascertain the optimal filter-wheel configuration for a particular imaging project.

Liquid-crystal tunable filters from Cambridge Research Instrumentation, Inc., (CRI) are also used. The visible liquid-crystal filter can be computer tuned to any wavelength in the 400-nm to 720-nm range with an optical bandwidth of 20 nm. A typical response curve is shown in Figure 2, below. The visible liquid-crystal filter is blocked at ultraviolet wavelengths but requires external IR blocking.

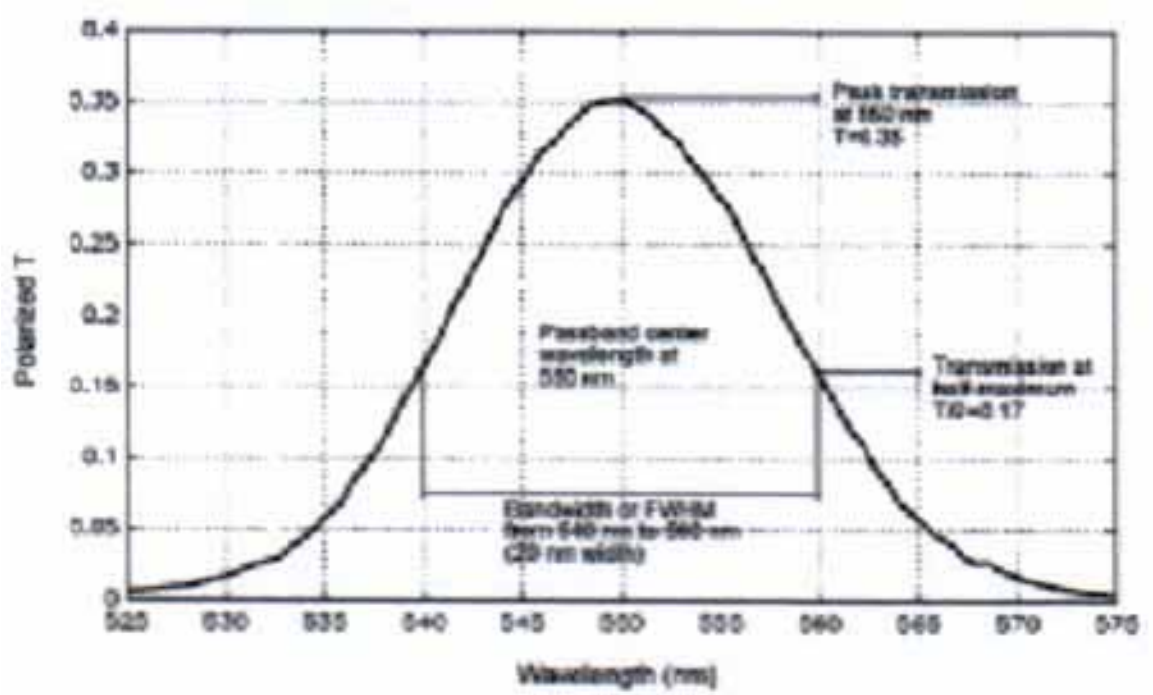

Figure 2. Typical response of the CRI visible tuneable filter. Curve by Cambridge Research Instrumentation, Inc.

The near-infrared (NIR) liquid crystal filter can be tuned to any wavelength from 650 nm through 1100 nm with an optical bandwidth of 7 nm and is blocked at visible and ultraviolet wavelengths. Both filters are typically tuned in steps of 20 nm. CRI also makes an RGB liquid-crystal filter which is used to produce standard color images.

Figure 3. Typical multispectral imaging system setup at Naj Tunich.

A typical system configuration is shown in Figure 3. This configuration was used for the multispectral imaging of the Maya cave drawings at Naj Tunich, Petén, Guatemala (Ware *et al*., 1999, 2000, 2001). Note the filter wheel mounted between the camera and the lens. The thickness of the filter wheel was set to preserve the normal focal length of the lens.

Lighting

Incident lighting can be provided by both quartz-halogen incandescent video lights and strobe units. The video lights use OSRAM quartz-halogen bulbs with a color temperature of 3400 K which is not as bright at short wavelengths as the 5500 K flash units. Both lighting systems provide about the same image illumination in the infrared, but the strobe units place a considerable lower heat load on the imaged scene. Video lights, however, allow effective use of both the camera exposure time setting and the gain setting to control the effective image brightness. They also provide constant illumination for real-time focus adjustment.

The relatively high power consumption of video lights make them difficult to use for extended periods of time on battery power such as was required to image the drawings at Naj Tunich. Here, ring and auxiliary strobe units were used for lighting to focus, set camera parameters, and for the final images. A ring-flash unit is mounted on the front of the lens in Figure 3.

Color temperature is not as important in multispectral imaging as it is in normal photography because of the relatively narrow wavelength range covered by a given image. This narrow wavelength range limits the total light energy reaching the sensor array and can become critical at short wavelengths around 400 nm and at long wavelengths approaching 1000 nm where the responsivity of the sensor array is low.

Calibration

Absolute responsivity calibration of over four million pixels in the sensor array from ultraviolet wavelengths through the near infrared is a formidable task. While uniformity of pixel response can more easily be verified, most imaging requirements can be met with a relative calibration using an average of multiple pixels. To this end, a Kodak gray scale card, where possible, is included in each image to record variations in incident lighting and allow relative calibration of reflectance vectors between scenes. This is especially important for spectral classification techniques. The gray scale also provides dimensional information when it is difficult to include a dimensional standard.

The focal length of a lens is a function of wavelength. While lenses are coated to minimize this variation at visible wavelengths, the narrow image bandwidth makes this effect still apparent, especially in the ultraviolet and the near infrared. The variation in focal length with image wavelength makes it necessary to individually focus each image and, in turn, causes the image magnification to vary as a function of the image wavelength. It is then difficult to accurately align the image cube for further processing. The image magnification (and image linearity) can be determined for each lens-filter combination by observing a target with a dimensionally accurate array of dots filling the field of view.

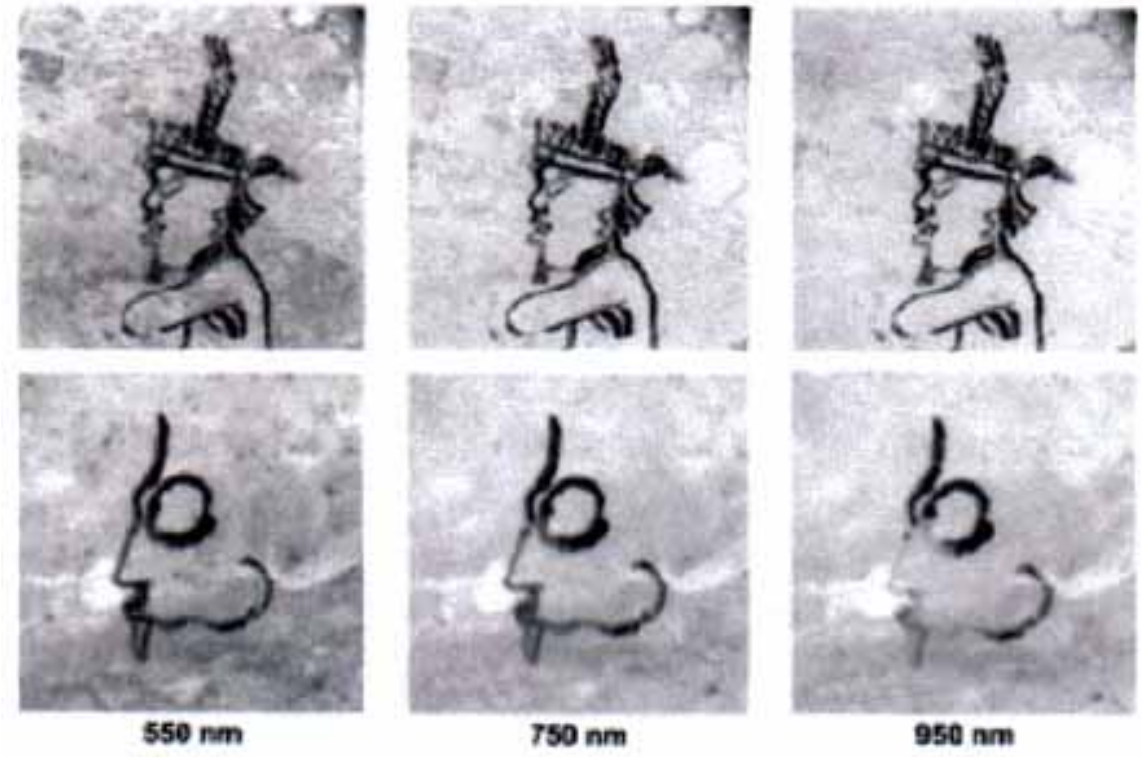

Figure 4. Multispectral images of Naj Tunich drawings 83 (top) and 62 (bottom).

Example Images

Multispectral images of two drawings from Naj Tunich are shown in Figure 4. Images of a royal dwarf (drawing 83) are shown along the top and images of a profile (drawing 62) are on the bottom[2]. The pigment used for drawing 83 is probably carbon based as it remains uniformly dark. Drawing 62 shows evidence of two different pigments, one of which fades into the infrared. Spectral classification reveals spots of the darker pigment in the faded area, perhaps as the result of an ancient touchup (Ware *et al*., 2000).

[2] The numbering system initiated by Stone (1995) for the drawings in the Naj Tunich corpus is used here.

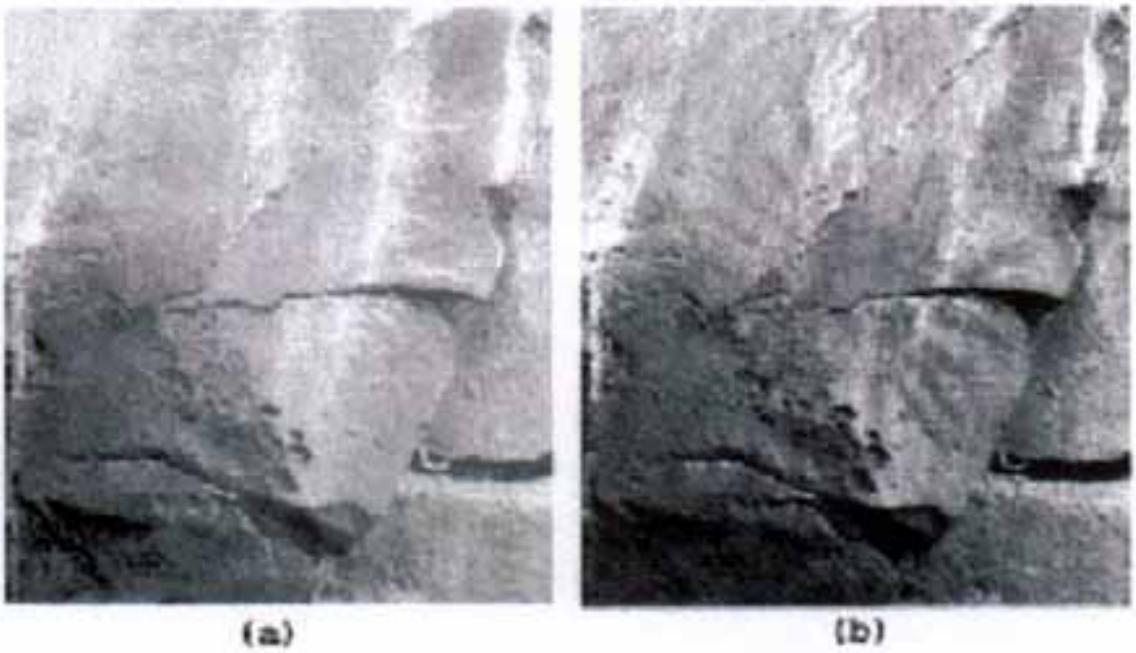

Figure 5. Multispectral images of Golondrinas drawing C10 at 1000 nm (a) and 550 nm (b).

Most pigments tend to fade into the infrared. This characteristic allows infrared images to "see through" pigments of paintings and ancient murals to reveal the carbon-based under drawing. This fading is illustrated by images of rock art drawing C10 at La Casa de las Golondrinas, Antigua Valley, Guatemala (Robinson and Ware, 2001). The rays which appear to be emanating from a sun are visible at 550 nm but disappear at 1000 nm. Figure 5 also illustrates the variation in image contrast with wavelength.

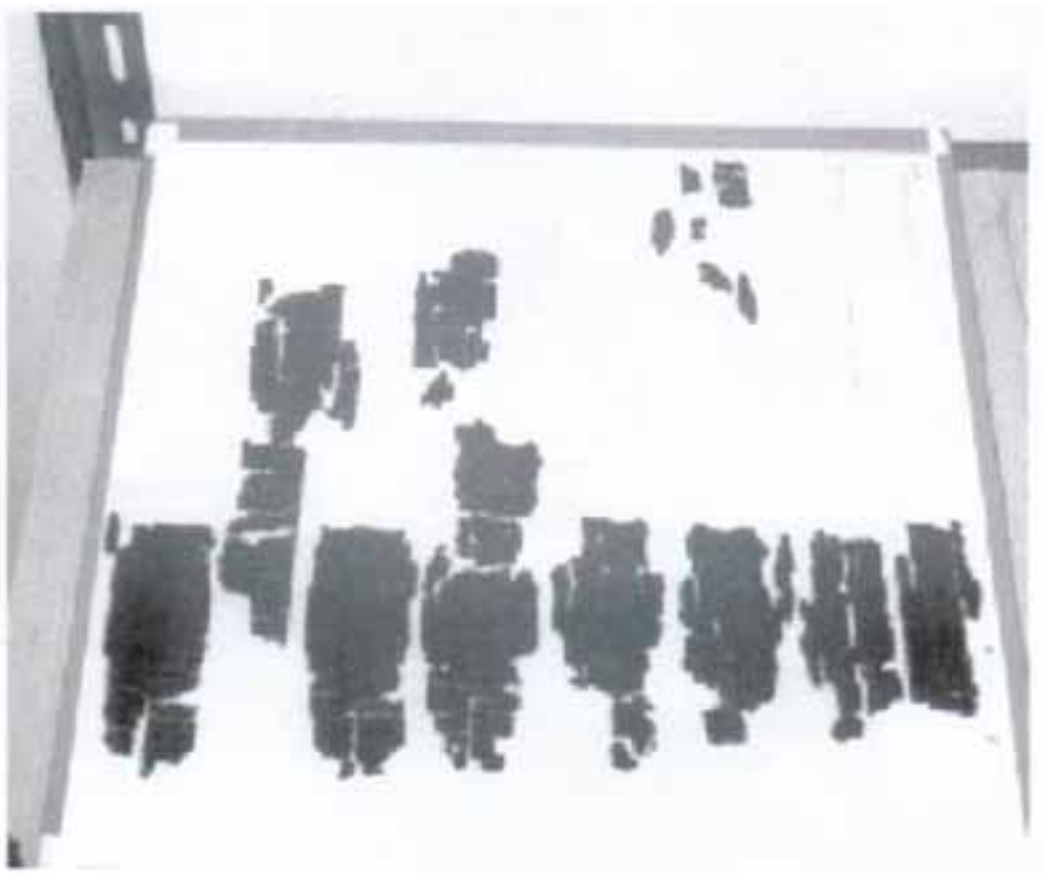

Figure 6. Plate 49 of the Petra Church Scrolls.

Figure 6 shows a black/white image of plate 49 of the Petra Church Scroll collection multispectrally imaged at the American Center of Oriental Research (ACOR) in Amman, Jordan. The writing on these carbonized scroll fragments is difficult to photograph because of the black-on-black characteristic. An image of the third fragment from the left along the bottom is shown in Figure 7. This image at 550 nm shows excellent contrast and is as clear as observing the original under a high-power microscope.

Figure 7. A multispectral image at 550 nm of a fragment on Plate 49 of the Petra Church Scrolls.

Spectral classification analysis has shown that the ink (probably carbon based) remains uniformly dark while the reflectance of the carbonized papyrus varies with wavelength (Ware *et al*., 2000). This causes wavelength for optimal image contrast to vary from fragment to fragment and within a fragment. By comparison, the carbonized scrolls from Herculaneum, Italy, uniformly exhibit excellent contrast in the 900-1000 nm region and poor contrast at visible wavelengths.

Conclusions

The archaeological multispectral imaging system described herein has been shown to effectively image a wide range of archaeological artifacts including ancient documents, carbonized scrolls, murals, drawings, rock art, and images on ceramics. The imaging system has been reliably transported to and used in environments ranging from the laboratory to museums, the jungle, and caves. The multispectral image data obtained, in concert with associated multispectral image processing, has exciting archaeological discoveries and understanding.

Acknowledgments

The design and fabrication of the multispectral imaging system described herein was supported by the College of Engineering and Technology at Brigham Young University. The Naj Tunich multispectral imaging research was supported by grants from the Foundation for the Advancement of Mesoamerican Studies, Inc., (FAMSI) and the Center for Advanced Study in the Visual Arts of the National Gallery of Art. The Golondrinas multispectral imaging research was supported by a grant from FAMSI. The Petra Church Scroll multispectral imaging project was conducted jointly by Brigham Young University and the American Center of Oriental Research (ACOR) in Amman, Jordan.

The mechanical design of the filter wheel was done by Dean Shaeffer of Space Dynamics Laboratory and Robert Perry of the BYU Research Machine Shop. Robert also led in the filter wheel fabrication, and in the design and fabrication of associated system hardware. Others who have assisted include Steven Booras, Ricky Fielding, Michael Ware, and Troy Johnson. The custom camera control software was written by Craig Lindstrom of eSage, Pleasant Grove, Utah.

List of Figures

All images are used by permission of Brigham Young University, Provo, Utah.

Sources Cited

Miller, Mary
1997 "Imaging Maya Art," *Archaeology* May/June, 74:3 pp. 34-40.

Belokon, William F., *et al*.
1977 *Multispectral Imagery Reference Guide*. Logicon Geodynamics, Inc.: Fairfax Virginia.

Roper Scientific, Inc.
2001 http://www.roperscientific.com/mega/pdfs/datasheets/megaplus/megaplus_4.2i.pdf, May 2001.

Cambridge Research & Instrumentation, Inc.
2001 http://www.cri-inc.com/data/pdf/5-061697.pdf, May 2001.

Ware, Gene A. and James E. Brady
1999 "Multispectral Analysis of Ancient Maya Pigments: Implications for the Naj Tunich Corpus," in *Center 19: Record of Activities and Research Reports June 1998-May 1999*. Washington D.C.: National Gallery of Art, Center for Advanced Study in the Visual Arts.

Ware, Gene A., Douglas M. Chabries, Richard W. Christiansen, James E. Brady, and Curtis E. Martin
2000 "Multispectral Analysis of Ancient Maya Pigments: Implications for the Naj Tunich Corpus." *Proceedings IEEE 2000 International Geoscience and Remote Sensing Symposium*, VI:2489-2491.

Ware, Gene A., James E. Brady and Curtis E. Martin
2001 "Multispectral Imaging and Spectral Classification of Naj Tunich Pigments," PICS 2001: *Proceedings of the 54th Annual Conference of the Society for Imaging Science and Technology*, April 22-25, Quebec, Canada.

Stone, Andrea
1995 *Images from the Underworld: Naj Tunich and the Tradition of Maya Cave Painting*. Austin: University of Texas Press.

Robinson, Eugenia J. and Gene A. Ware
2001 "Multi-spectral Imaging of La Casa de las Golondrinas Rock Paintings." Final Report submitted to FAMSI.

Ware, Gene A., Douglas M. Chabries, Richard W. Christiansen, and Curtis E. Martin
2000 "Multispectral Document Enhancement: Ancient Carbonized Scrolls." *Proceedings IEEE 2000 International Geoscience and Remote Sensing Symposium*, VI:2486-2488.

Multi-spectral Imaging of La Casa de las Golondrinas Rock Paintings

Appendix B. Unsupervised Clustering for Data Reduction and Analysis of Multispectral Archaeological Images

by Curtis E. Martin, U.S. Air Force Academy, Colorado, and Gene A. Ware, Brigham Young University

Table of Contents

Abstract

A vector quantization approach to performing cluster analysis of multispectral image data is proposed. A distortion measure based on the shape of spectral reflectance vectors is suggested, and reasons for this choice are set forth. The algorithm is used to perform both intra- and inter-image cluster analyses of multispectral images of archaeological cave paintings. Within single images, the algorithm successfully separates the pigment from the stone background, and further distinguishes between two types of pigments found in the same image. When clustering data from multiple images, the algorithm identifies drawings that may have been created with the same pigment, while simultaneously identifying other drawings that were likely drawn with different pigments. Challenges involved with using this approach in general cluster analysis are discussed, and possible solutions for these challenges are given. Although these challenges are non-trivial, the preliminary results obtained thus far seem promising enough to encourage further study of the proposed technique.

Introduction

Multispectral imaging has been used in many remote sensing applications over the past several years, most commonly in satellite imaging of the earth for various earth-monitoring purposes. In recent years, however, the range of applications for multispectral imaging has been greatly expanded. Scientists have turned to multispectral imaging to obtain greater understanding of the galactic center (Kirkland, Baker, and Ware, 2001), to retrieve texts from ancient mutilated documents (Knox *et al*., 2001, Ware *et al.*, 2000), and to perform non-destructive analysis of pigments in cave paintings far beneath the surface of the earth (Ware, Brady, and Martin, 2001).

One of the most important tasks in image processing is image segmentation–breaking an image into constituent parts to find the items of interest within the image. While conventional image segmentation typically uses spatial structure to isolate different parts of an image, multispectral imagery provides an additional axis along which discrimination can be made–the spectral axis. In fact, the ability to perform spectral discrimination is precisely the reason why multispectral imaging systems are typically used where they are. In virtually every application of multispectral imaging, the typical first interest of the investigator is to find the regions of the image that contain unique spectra, as these correspond to areas in the image subject that have different chemical compositions.

This paper describes a technique for multispectral image segmentation that uses a vector quantization algorithm to group the pixels of the multispectral image based on similarities in their measured spectra. The vector quantization algorithm is briefly described, and then its application as a clustering algorithm for multispectral image segmentation is explained. Results from applying the algorithm to multispectral archaeological imagery are then presented. A brief discussion of some of the challenges involved in using this approach for multispectral image segmentation follows, and some suggestions for overcoming these challenges are offered. Although at present there remain unresolved challenges that require care in the interpretation of results, the initial results obtained using this approach seem promising enough to warrant effort in resolving the difficulties.

Vector Quantization

Vector quantization (VQ) is a process of coding a source signal, usually a sequence of vectors, using a fixed set (or codebook) of prototype vectors and a rule for associating each input vector with one of the codebook vectors. Using the association rule, the coding process is accomplished by replacing each input vector with the index to the codebook vector that best represents it. To reconstruct the signal, each coded index is replaced with the appropriate vector from the codebook. Because each vector in the reconstructed signal is not an exact replica of the original input vector, vector quantization introduces some error (or distortion) into the signal. This error is measured by means of a *distortion measure*–a

mathematical formula that provides a quantified assessment of the difference between an input vector and the codebook vector selected to represent it.

Most often, it is desirable to minimize the overall expected distortion imposed by a VQ system. A rule that will accomplish this goal is to pick, for each input vector, the prototype from the codebook that produces the minimum distortion for that vector. Given any set of unique codebook vectors, this minimum distortion association rule produces a *partition* of the input vector space. That is, the input space is divided into a set of non-overlapping cells, each around a different codebook vector, in such a way that the source vectors within a given cell are closer to that prototype vector (in the sense of the distortion measure) than to any other member of the codebook. Conversely, given any partition of the input space, a minimum-distortion codebook may be constructed by finding a vector in the center of each cell of the partition, so that the average distortion incurred by replacing each vector in the cell by the proposed prototype is minimized. Gray *et al*. have shown that for all useful partitions and a large set of distortion measures, such a set of minimum-distortion codebook vectors can always be constructed (Gray, Keiffer, and Linde, 1979).

Recognizing that a minimum distortion partition can be constructed for virtually any set of codebook vectors, and that a minimum distortion codebook can be obtained for virtually any useful partition, Linde, Buzo, and Gray (1980) proposed an efficient iterative algorithm (hereafter referred to as the LBG algorithm) for designing an optimal vector quantizer for a given signal source. The LBG algorithm is initialized by arbitrarily choosing an initial codebook with the desired number of codebook entries. The first iterative step is to determine the minimum-distortion partition of the input space for this initial codebook. Then, the algorithm updates the codebook, replacing it with the set of prototypes that minimizes the distortion for the partition found in the first step. The algorithm continues, alternatively updating first the partition and then the codebook, until the overall distortion obtained by the partition does not change between iterations more than a user-specified threshold. Conditions necessary to guarantee convergence of the algorithm to a "good" quantizer, which are relatively mild (Linde *et al*., 1980) are formally stated by Gray *et al*., (1979).

To process multispectral imagery based on spectral content, the multi-spectral data are treated as a spatial distribution of spectral reflectance vectors $\vec{x}_{ij}$. The indices *i* and *j* maintain the spatial location of each vector in the image, while the vector itself contains the spectral reflectance of the material located at that position in the subject. (Note that although we are restricting our discussion to reflective subjects, there is no reason to suspect that the same techniques to images of emissive sources, e.g. astronomical images.)

In segmenting a multispectral image, the primary goal is to isolate clusters of pixels from each other that correspond with portions of the subject that have characteristic spectra. This process is essentially one of partitioning the data in spectral reflectance space–we seek clusters that are unique to the various constituent materials of the imaged subject. Once the spectral reflectance vectors are assigned to clusters, the spatial distribution of these constituent materials

throughout the image can be examined by looking at how the clusters are distributed through the image.

Although the primary focus of the LBG algorithm is on developing a codebook that yields minimum distortion in reconstructing the input signal, a natural byproduct of the algorithm is the partition of the input space that accompanies the optimum codebook. Thus, while the clusters (i.e. partition) obtained by the LBG algorithm may not correspond directly with the "naturally occurring" clusters of the data, it seems reasonable to at least try using the LBG algorithm as a means for cluster analysis of multispectral imagery.

Two features of the LBG algorithm make it more attractive for evaluation as a clustering tool for multispectral data. First, it requires very little in the way of assumptions regarding the distribution of the data. Because of the high dimensionality, it is generally difficult to assume much in terms of how multispectral data will be distributed in spectral reflectance space. However, physical intuition provides at least a possibility that the data are in fact distributed in some sort of cluster form. The second feature that makes LBG attractive for clustering multispectral data is its generality with respect to the distortion measure. This allows the selection of a distortion measure for the clustering process that has greater intuitive and physical appeal than the often-used squared-error distortion measure.

Clustering by Spectral Shape

When choosing a distortion measure for use in either vector quantization or cluster analysis, it is important to choose a measure that is relevant to the data. In the case of multispectral data, particularly data collected under non-uniform lighting conditions, an ideal distortion measure will be sensitive to differences in spectral shape, while being relatively insensitive to variations in the overall light intensity. This is because the objective in multispectral cluster analysis is to find groups of pixels that come from similar materials in the imaged subject. Because different materials generally may be uniquely characterized by their spectral reflectance, pixels representing a given material in the subject would be expected to have similar spectral reflectance vectors. Variations in illumination intensity would tend to raise and lower this shape as a whole, but the relative shape would remain constant for each material.

Thinking of multispectral data vectors as position vectors in n-dimensional Euclidean space, each possible spectral shape corresponds to a specific direction in that space (n corresponds to the number of elements in each reflectance vector). Increasing the magnitude of the illumination, then, would increase each spectral component by a constant factor, which would simply change the length of the resulting vector without affecting its direction. With this thought in mind, given a multispectral data vector x and a cluster prototype y, the difference (or distortion)

between these two vectors in the n-dimensional spectral reflectance space may be computed in terms of the angle between their directions as

$$d(\vec{x},\vec{y}) = 1 - \cos(\theta), \qquad (1)$$

where θ is the angle between the vectors and . With this particular formulation, vectors that have the same shape (i.e., lie along the same direction) will have zero distortion, regardless of differences in illumination, while those that are reflections of each other will have a maximum distortion of two.

Because of its relationship to the angle between the two vectors in spectral reflectance space some have dubbed this distortion measure the "spectral-angle measure," (SAM) (Kruse, 2000). In addition to its strong intuitive appeal for use in clustering multispectral data, this distortion measure is also quite simple computationally. Using vector analysis, a simpler computational form of Eq. (1) may be stated as

$$d(\vec{x},\vec{y}) = 1 - \hat{x} \cdot \hat{y}, \qquad (2)$$

where and ŷ are unit vectors obtained by dividing each vector by its respective magnitude. Thus, in preparing multispectral image data for cluster analysis using the spectral-angle measure in the LBG algorithm, the last preprocessing step is to normalize each pixel's spectrum vector by dividing by its magnitude. In turn, each time the codebook vectors are recomputed in the LBG algorithm, they must be re-normalized to ensure they remain unit vectors as well. Incorporating the spectral angle measure into the LBG algorithm produces the proposed clustering algorithm, which we shall refer to hereafter as the SAM/LBG algorithm.

Because it uses an index array to keep track of the partitioning of the training data throughout the VQ design process, the LBG algorithm can provide this array as an output that tells the cluster to which each pixel is assigned. By assigning a unique color to each cluster index, this index array can be used to create a false-color image of the clustering results, which is useful in assessing the value of the results obtained.

Experiments

Multispectral Image Data Set

The SAM/LBG algorithm was applied to a set of multispectral images of archeological artifacts (cave paintings). The images were taken using a Kodak Megaplus Camera (Model 4.2i), with spectral definition obtained via a set of optical interference filters mounted in a filter wheel. The complete set of filters had center wavelengths ranging from 400 through 1000 nm in 50 nm increments; the bandwidth of each filter was 40 nm. Ring and auxiliary strobe units provided the illumination source for the imaging (Ware, Chabries, and Baker, 2001). Only the 450 through 950 nm images were used for the analysis reported herein.

Data Set Preparation

Prior to performing the LBG algorithm with the multispectral image data, several preprocessing steps were required, including cropping each image to include just the painting of interest, performing a band-to-band registration process to ensure (as nearly as possible) that each pixel in every band represented the same part of the subject, and performing an illumination equalization process to account for different illumination conditions between the various bands. A standard gray-scale card included in each spectral band image facilitated the last of these processes. After completing these steps, each spectral reflectance vector was normalized to unit magnitude in preparation for clustering.

Data Clustering Tasks

Two data clustering tasks were attempted using the SAM/LBG algorithm. In the first task, the algorithm was applied to individual multispectral images to ascertain if it would make a clean separation between the pigmented pixels in the drawing and those of the background rock. In the second task, a composite multispectral "image" was made by gathering the measured spectra of pigmented "swatches" from several drawings, and the algorithm was applied to this composite data set to see if it would suggest any interesting similarities or differences between the spectral reflectance vectors of the various pigments in the different drawings.

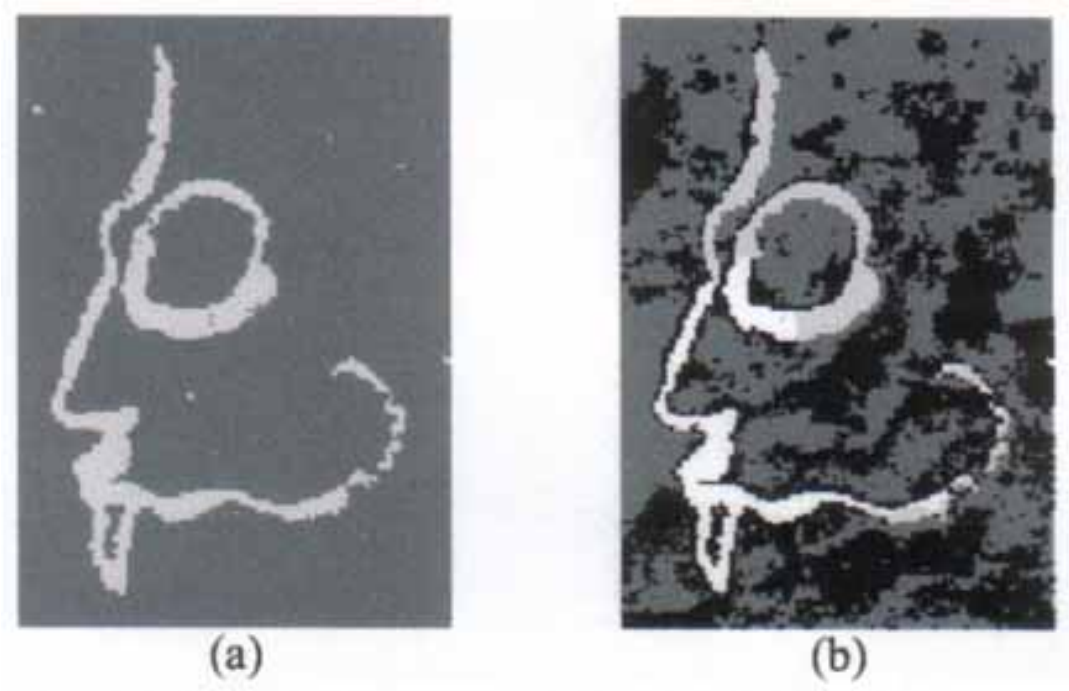

Figure 1. SAM/LBG Clustering results for Drawing 62: (a) two clusters, (b) four clusters.

Results and Analysis

Task 1: Intra-Image Clustering

The results of the LBG clustering algorithm for the first task are shown for two drawings in Figure 1, above, and Figure 2, below. For both of these drawings, the initial prototypes for the four-cluster runs were obtained by adding and subtracting a small random vector to each of the final prototypes from the two-cluster runs. These results appear to be quite favorable–in both drawings the two-cluster run produces a reasonable separation of pigment from rock, and the four-cluster run further subdivides the rock and pigment groups into two sets each. Close inspection of the spectra for these drawings reveals that at least two distinct types of pigments actually do exist in each drawing.

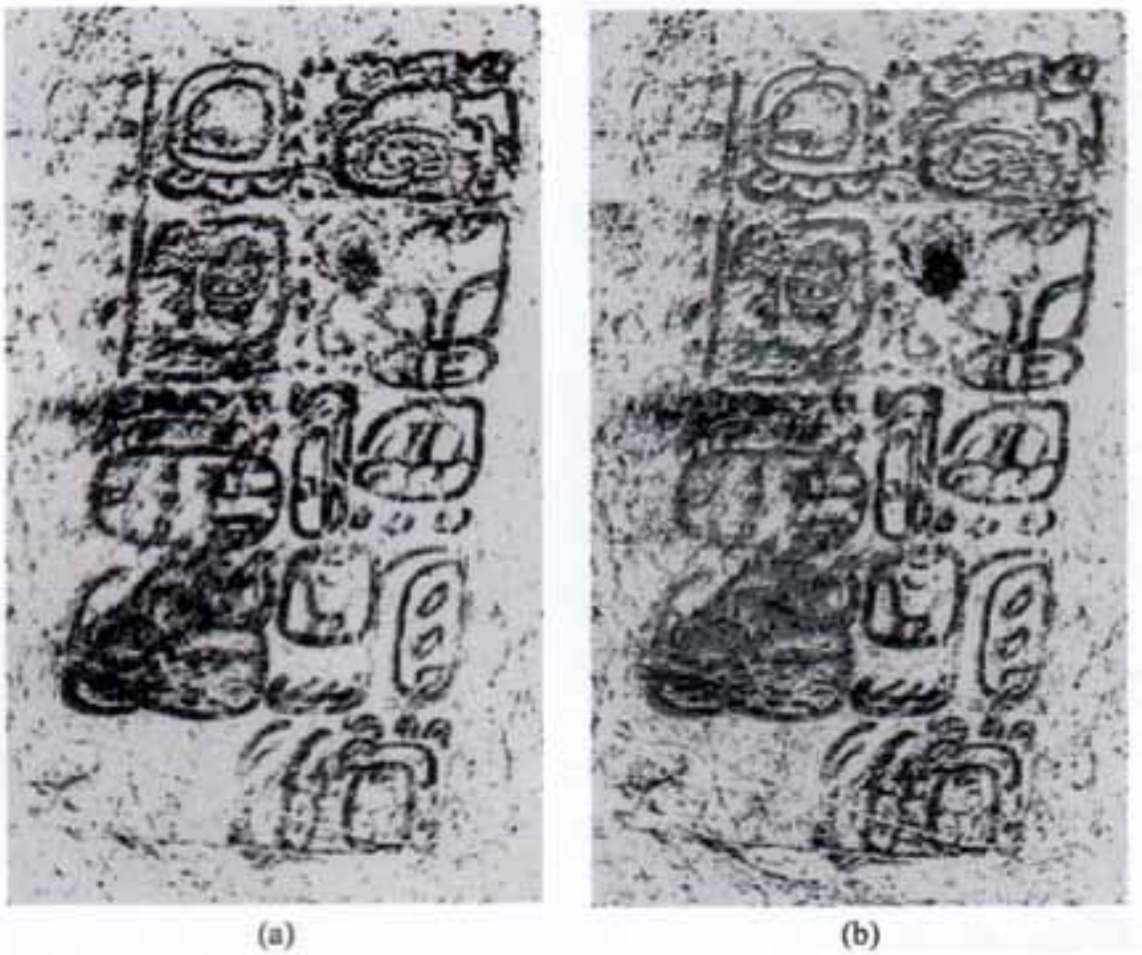

Figure 2. SAM/LBG Clustering results for Drawing 62: (a) two clusters, (b) four clusters (represented by four different gray-scales).

Task 2: Inter-Image Clustering

The second task was intended to look for similarities and differences in pigment spectra across several drawings. To accomplish this task, the multispectral data from sixteen 100x100 pixel swatches from pigmented areas of fourteen drawings were placed adjacent to one another to form a composite multispectral "image." Sixteen arbitrary vectors were chosen as initial codebook entries, and then the SAM/LBG algorithm was applied to the multispectral data set sixteen times. On the first run, the algorithm looked for sixteen clusters, and on each successive run, the number of desired clusters was reduced by one. This multiple-run scheme was adopted because there was no simple way of knowing in advance how many different types of pigments had been selected, and we wanted to determine how the clusterings would change as fewer and fewer clusters were sought.

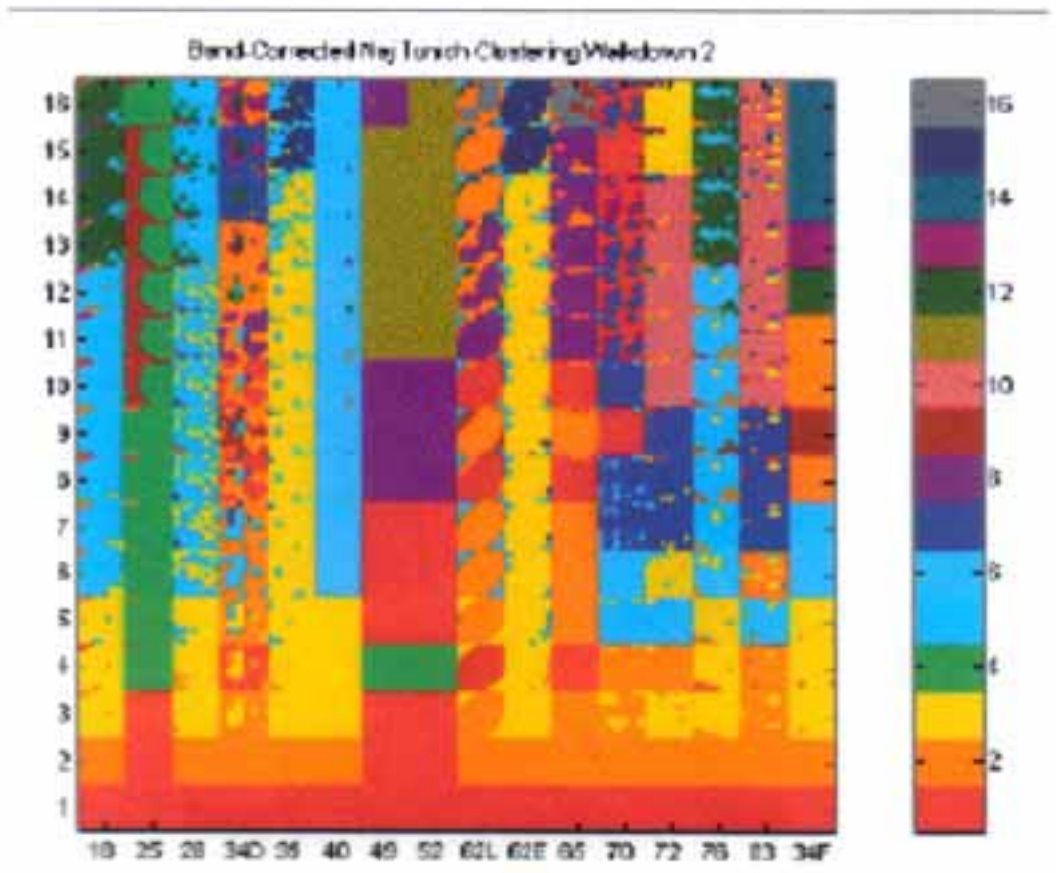

Figure 3. Sixteen runs of the SAM/LBG algorithm applied to a composite image of pigment samples. Each row corresponds to results obtained while seeking a different number of clusters.

Figure 3 shows the results obtained by these sixteen runs of the SAM/LBG algorithm on the composite multispectral image of sixteen pigment swatches.

While it is somewhat difficult to distinguish all sixteen clusters in the top row of this gray-scale representation, note that the columns labeled as 49 and 52 are the same shade of gray in each row except for row 16, while the columns labeled 62L and 65 are essentially the same gray level in each row from row 11 all the way down to row 1. (The color changes from row to row as a consequence of the somewhat arbitrary assignment of color to cluster index. The important thing to note is that the two columns in each pair are the same color in each row mentioned.) These results imply that the spectra from these different pigment samples are so similar that these drawing pairs (49/52 and 62L/65) may in fact contain the same pigments (or at least very similar pigments).

Discussion

While the results obtained with the SAM/LBG algorithm appear to be quite reasonable, several issues merit some serious consideration.

Split or Clumped "Natural" Clusters

The first issue to consider is the fact that the LBG algorithm (and, hence, our new algorithm) is designed to find exactly the same number of clusters as the user requests. If it has to subdivide a "natural" cluster or group two such clusters together to produce the requested number of clusters, it will do so. For example, if a user attempts to find four clusters in a set of data that lies naturally in three separate clusters, the algorithm will somehow split one of the three clusters to form the fourth cluster. Similarly, if the user asks for two clusters where there are three natural groups in the data, the algorithm will be forced to cluster some or all of one group with one or both of the remaining groups. Finally, it is not difficult to imagine a distribution in which the algorithm would split two "natural" groups in half, then regroup the halves, resulting in two "half-breed" clusters. All of these possible errors arise as a consequence of the fact that the LBG algorithm is designed to minimize reconstruction error from the VQ coding process, not to find the set of "natural" clusters in the data. As a result, trying to use the LBG algorithm to perform cluster analysis may actually be fraught with error.

Two ways to overcome this difficulty have been briefly explored, although results sufficient to draw solid conclusions have not yet been obtained. The first approach is that illustrated in Task 2 above. While it is impossible to visualize the groups of data in 6-dimensional space, by conducting a carefully controlled procedure that gradually reduces the number of clusters obtained from a constant set of starting points, it is possible to gain some insight into how different parts of the data are related to each other. The second approach, inspired by Martinetz and Schulten (1980), involves measuring the density of training data between adjacent prototypes to identify cases where natural clusters may be split.

Local vs. Global Minima

Another issue to consider is whether the algorithm converges on the absolute minimum point, or gets stuck at a local minimum. As there really is nothing to prevent the algorithm from converging to a local minimum, the solution produced depends somewhat on the initial condition that is chosen. Linde, Buzo, and Gray anticipated this problem and proposed a solution for it (1980), but the effects of their proposed solution on a cluster analysis application of their algorithm have yet to be explored.

Summary

We have shown how the algorithm developed by Linde, Buzo, and Gray for designing an optimal vector quantizer may be adapted for use in cluster analysis of multispectral image data. The algorithm is attractive because it does not require extensive assumptions as to the true distribution of the data, and it also may be implemented with a wide range of distortion measures. We have discussed the appropriateness of the spectral angle measure as a distortion measure for use in clustering multispectral image data, and we have shown that this measure can be used within the framework of the LBG algorithm to obtain apparently reasonable separations of pigments from unpainted rocks. Our results also demonstrate that finer discriminations can be made, as we have shown several examples where similarities between pigments, as well as differences, are identified by the algorithm.

Although these results are promising, we acknowledged that this approach may be limited in its usefulness in the cluster analysis of multispectral data. We have identified two difficulties that may arise from using an algorithm for designing a vector quantizer as a tool for cluster analysis, and we have mentioned some ideas for addressing these difficulties. Further study will be required to ultimately answer whether or not these difficulties may be successfully overcome. However, the results obtained thus far seem compelling enough to motivate this requisite study.

Acknowledgments

The Naj Tunich multispectral imaging research project was supported by grants from the Foundation for the Advancement of Mesoamerican Studies, Inc., (FAMSI) and the Center for Advanced Study in the Visual Arts of the National Gallery of Art.

All images are used by permission of Brigham Young University, Provo, Utah.

List of Figures

Sources Cited

Kirkland, J.S., D.J. Baker and G.A. Ware

2001 "Principal Components Data Fusion of Infrared Telescope Multispectral Images of the Galactic Center," Presented at *SCI2001,* Orlando, FL.

Knox, K., *et al.*

2001 "Multispectral Imaging of the Archimedes Palimpsest," *Proceedings of the 2001 Annual Conference of the Society for Imaging Science and Technology: Image Processing, Image Quality, Image Capture, Systems Conference,* pp. 206-210.

Ware, G.A., *et al.*

2000 "Multispectral Document Enhancement: Ancient Carbonized Scrolls," *Proceedings IEEE International Geoscience and Remote Sensing Symposium,* VI:2486-2488.

Ware, G.A., J.E. Brady and C.E. Martin

2001 "Multispectral Imaging and Spectral Classification of Naj Tunich Pigments,"*Proceedings of the 2001 Annual Conference of the Society for Imaging Science and Technology: Image Processing, Image Quality, Image Capture, Systems Conference,*pp. 211-214.

Gray, R.M., J.C. Keiffer and Y. Linde

1979 "Locally Optimal Block Quantization for Sources without a Statistical Model," Stanford University Information Systems Lab Technical Report No. L-904-1, May, Stanford, CA.

Linde, Y., A. Buzo, and R.M. Gray

1980 "An Algorithm for Vector Quantizer Design," *IEEE Trans. on Communications,* Vol. COM-28, pp. 85-95.

Kruse, F.A.

2000 *Introduction to Hyperspectral Data Analysis,* Boulder: Analytical Imaging and Geophysics.

Ware, G.A., D.M. Chabries and D.J. Baker

2001 "Multispectral Imaging for Archaeology," Presented at *SCI2001,* Orlando, FL.

Martinetz, T. and K. Schulten

1980 "Topology Representing Networks," *Neural Networks,* Vol. 7, pp. 507-522.